Missouri University of Science and Technology
Scholars' Mine

Materials Science and Engineering Faculty Research & Creative Works

Materials Science and Engineering

01 Jan 2023

Reduction Of Iron-Ore Pellets Using Different Gas Mixtures And Temperatures

Yuri Korobeinikov

Amogh Meshram

Christopher Harris

Olexandr Kovtun

et. al. For a complete list of authors, see https://scholarsmine.mst.edu/matsci_eng_facwork/3193

Follow this and additional works at: https://scholarsmine.mst.edu/matsci_eng_facwork

Part of the Materials Science and Engineering Commons

Recommended Citation

Y. Korobeinikov et al., "Reduction Of Iron-Ore Pellets Using Different Gas Mixtures And Temperatures," *Steel Research International*, Wiley, Jan 2023.
The definitive version is available at https://doi.org/10.1002/srin.202300066

This Article - Journal is brought to you for free and open access by Scholars' Mine. It has been accepted for inclusion in Materials Science and Engineering Faculty Research & Creative Works by an authorized administrator of Scholars' Mine. This work is protected by U. S. Copyright Law. Unauthorized use including reproduction for redistribution requires the permission of the copyright holder. For more information, please contact scholarsmine@mst.edu.

steel research international
www.steel-research.de

Reduction of Iron-Ore Pellets Using Different Gas Mixtures and Temperatures

Yuri Korobeinikov, Amogh Meshram, Christopher Harris, Olexandr Kovtun, Joe Govro, Ronald J. O'Malley, Olena Volkova, and Seetharaman Sridhar*

Direct reduction of iron ore (DRI) is gaining an increased attention due to the growing need to decarbonize industrial processes. The current industrial DRI processes are performed using reformed natural gas, which results in CO_2 emission, although it is less than carbothermic reduction in the blast furnace. Carbon-free reduction may be realized through the utilization of green H_2 as a reducing agent, in place of natural gas. Herein, the effects of various gas mixtures and temperature on the reduction kinetics of the hematite iron-ore pellets are focused on in this work. Pellets are reduced at 700, 800, 850, and 900 °C in hydrogen and using various gas mixes at 850 °C. Morphology of the pellets is investigated with the help of scanning electron microscopy and mercury intrusion porosimetry. The effects of temperature and gas composition on the reduction kinetics and porosity of the pellets are discussed. A notable effect of reduction rate on the internal structure of the pellets is detected, slower reduction rate yielded bigger pores offsetting the gas composition. Higher temperature results in coarser pores and higher porosity. Increase of CO content in the gas mix also leads to bigger pore size.

1. Introduction

In the last few decades climate change has started to adversely impact humanity, wildlife, and economics. Iron- and steelmaking process is among the major industrial CO_2 sources. Steelmaking is responsible for about 7% of all anthropogenic emissions of CO_2.[1] This poses a clear challenge for the steel industry to reduce CO_2 emissions. In the entire steelmaking process, the highest share of energy consumption and subsequent CO_2 emissions belong to the iron-ore reduction step using carbon as a reducing agent.[2–4] Historically, coal was the most economically efficient reducing agent for converting iron oxides into metallic iron. After the development of fracking, natural gas derived from shale could be economically more advantageous[5] in some geographic locations. However, global targets to curb the CO_2 emissions renders both coal and natural gas unsustainable for steelmaking, unless carbon capture, utilization, and storage (CCUS) is deployed at an industrial scale.

Apart from the extreme effects of climate change, iron-ore reduction is very energy intensive. Due to this high-energy demand in the form of feedstock or process heat, the ironmaking process is inevitably bound toward the question of affordability and availability of energy sources. As was mentioned earlier, the most economical way to produce iron from iron ore to date is the use of coking coal (coke) in blast furnaces (BFs). The BF has evolved through history and has become a highly efficient reactor in terms of both capacity and quality, but it is still dependent on coke to produce iron.

Alternative ironmaking technologies have existed for decades. The most successful among them is the natural-gas-based MIDREX shaft furnace technology.[6] The closest rival is ENERGIRON process[7] developed from a partnership between Tenova and Danieli, which operates at higher pressures and does not require an external reformer for natural gas. The advantage of the shaft furnace solid-state reduction is that the system is not overspecialized on iron-ore quality and on natural gas source. Unlike BF, shaft reactors in principle can work on a variety of hydrocarbon sources ranging from natural gas up to gasified low-quality coals in any proportions. Unfortunately, natural gas has two drawbacks: 1) it is unevenly available on the earth, although global natural gas market has significantly grown the last decade; and 2) its use is associated with CO_2 emissions, albeit it is less in comparison to coal. In the USA, natural gas is relatively cheap since the deployment of fracking technology to utilize the shale gas, which is available in an abundance.

A radical solution for decarbonization of ironmaking industry can be achieved with the use of hydrogen as a primary reduction

Y. Korobeinikov, A. Meshram, S. Sridhar
Ira A. Fulton School of Engineering
Arizona State University
Tempe, AZ 85281, USA
E-mail: ikorobei@asu.edu

C. Harris
Voestalpine AG
Linz, Austria

O. Kovtun, O. Volkova
Institute of Iron and Steel Technology
Freiberg University of Mining and Technology
Freiberg 09599, Saxony, Germany

J. Govro, R. J. O'Malley
Kent D. Peaslee Steel Manufacturing Research Center (PSMRC)
Missouri University of Science and Technology
Rolla, MO 65409, USA

The ORCID identification number(s) for the author(s) of this article can be found under https://doi.org/10.1002/srin.202300066.

DOI: 10.1002/srin.202300066

 © 2023 Wiley-VCH GmbH

gas in shaft reactors. About 99% of industrial hydrogen supply today originates from the natural gas, coal, and oil reforming, which is associated with a considerable carbon footprint.[8] In this production route, 1 kg of H_2 results in 10 kg of CO_2 as a waste.[8] Such H_2, if carbon dioxide is subsequently captured and not released to the atmosphere, is labeled as "blue". Another option of H_2 production is the electrolysis of water where the CO_2 emissions can be effectively lowered in the case of renewable electricity use. This process is 2–3 times more expensive and currently is in the early stage of market adoption accounting for about 0.03% of total H_2 supply in 2020.[8] Nevertheless, both the capacities of renewable energy generation and water electrolysis are growing with time and excessive energy generation must be somehow utilized. Electrolysis of hydrogen for metallurgical applications looks like a reasonable solution which will not require a massive investment in H_2 storage and distribution infrastructure.

The combination of hydrogen and natural gas as a reductant in the shaft reactor may offset the disadvantages of both gases for commercial direct reduction of iron ore (DRI) production. Hydrogen can be used in the event of peak renewably sourced power generation with nearly negative electricity prices. Natural gas can be used as part of the mix or as a complete substitute when 100% H_2 for DRI production is not economical. It is interesting to notice that both shaft reduction technology rivals—Midrex, and Tenova and Danieli—are now offering options of reactors with high H_2 concentration.[9] It is already well understood that increasing the amount of green H_2 produced with renewable electricity in the direct reduction gas feed improves the carbon footprint drastically and eliminates the need of carbon removal from the off gas. On the contrary, if H_2 is produced with natural-gas- or coal-based electricity, carbon footprint of the process becomes worse than pure natural-gas-driven reduction.[9] These cases are valid for typical EU or USA grids. Therefore, application of H_2 in the steelmaking process should be made with careful consideration of the source of H_2.

Iron oxides can be reduced in different ways. According to the Richardson–Ellingham diagram[10] all the elements laying below the $Fe + O_2 = FeO$ line can work as a reduction agent at certain temperatures (**Figure 1**). However, most of options are noneconomical in the foreseeable future, except for two gases, CO and potentially H_2.

Extensive details of the topic of H_2 gas direct reduction of iron ores (DRI) can be found in the recent reviews of Spreitzer and Schenk,[11] Patisson and Migraux.[12] Heidari et al.[13] reviewed the kinetics studies of iron-ore reduction. Ghadi et al.[14] made an explicit review of models for pellets reduction. According to Baur–Glässner diagram (**Figure 2**), H_2 is more efficiently utilized at higher temperatures where higher oxidation degrees of gas allow existence of metallic iron. As for CO, after about 600 °C, efficiency of gas-utilization decreases. However, at higher temperatures, kinetics of reduction plays a more important role in reaction. Therefore, the most modern natural-gas-based MIDREX plants tend to operate in a range of 900–950 °C, where the limiting factor is the softening and sintering of the DRI pellets at higher temperatures.

H_2 as a potential reducing agent for iron ores was quite intensively investigated since 1960s. Among the most notable works related to the iron-ores reduction can be named the book of L. von Bogdandi and H.-J. Engell.[15] Since then, kinetics of

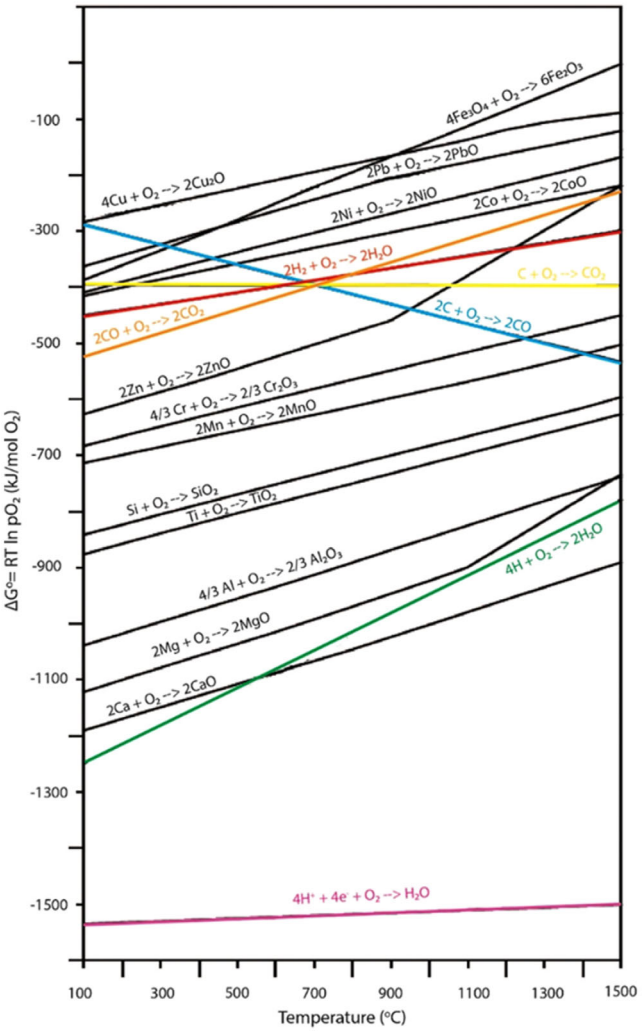

Figure 1. Ellingham type diagram of metal oxides. Reproduced with permissions.[46] Copyright 2022, Springer.

iron-ore reduction has been extensively investigated.[16–25] Various H_2–CO mixes[26–28] were investigated as well. It was already established in the 1960s that the main rate controlling mechanisms are chemical reaction and diffusion through the Fe–ash layer whose resistance increases as the reduction process proceeds. Gas-film resistance is usually negligible at the gas flow rates observed in industrial conditions.

It is well established that an increase of H_2 share in the reduction gas mixture leads to higher reduction rate of the iron oxides.[11,29,30] The same effect was reported for increases in temperature and partial pressure.[11,29] Higher porosity of the pellet improves the gas penetration into the unreacted core, and therefore it enhances reduction rate as well.[11,31] Tortuosity is negatively affecting the reduction rate of the iron-ore pellet.[29,30] In the recent time, some studies were performed on the topic of iron-ore pellets structure evolution. Ma et al.[32] studied microstructure evolution of commercial pellets reduced with hydrogen at 700 °C. Scharm et al. studied the evolution of pellet structure and porosity as a function of temperature between 800 and 1100 °C and H_2–CO ratio.

© 2023 Wiley-VCH GmbH

1869344x, 0, Downloaded from https://onlinelibrary.wiley.com/doi/10.1002/srin.202300066 by Missouri University Of Science, Wiley Online Library on [16/08/2023]. See the Terms and Conditions (https://onlinelibrary.wiley.com/terms-and-conditions) on Wiley Online Library for rules of use; OA articles are governed by the applicable Creative Commons License

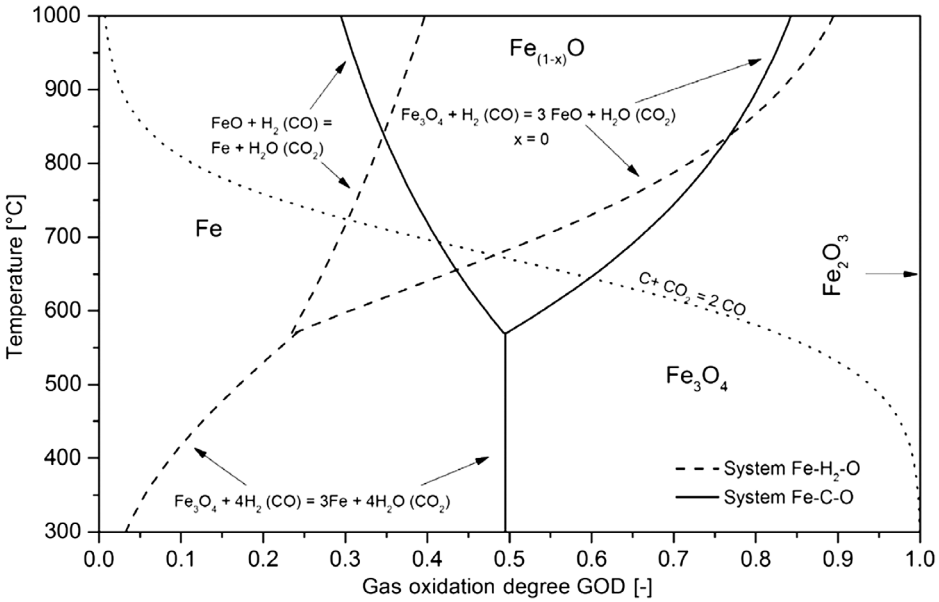

Figure 2. Baur–Glässner diagram for the Fe–O–C and Fe–O–H systems, which includes also Boudouard equilibrium for 1 bar pressure and carbon activity of 1. Reproduced with permission.[11] Copyright 2019, Springer.

This study is accomplished as a part of the grid interactive hydrogen steelmaking (GISH) project, which aims at evaluating a reactor which can switch from H_2 to natural-gas-based reduction in a flexible manner. Although the kinetics of iron-ore reduction is not of novelty as such, they are always specific to individual sample types and therefore experimental data is valuable for validation of reduction models for specific pellet types. Another feature of present research is the use of relatively big sample size which delivers results closer to the industrial reactor scale. The aim of this article is to report experimental investigations of reduction kinetics of commercial iron-ore pellets reduced at various temperatures using H_2 and using various gas mixtures and their effect on the final pellet structure. A careful study of internal structure of pellets with the application of scanning electronic microscopy (SEM) and mercury intrusion porosimetry (MIP) should give detailed information on the effects of gas mix and temperature. Kinetics and porosity data were previously used for developing model of single-pellet reduction[33,34] and is used for developing a new reactor-scale model. One of the ultimate goals of the GISH project is to develop a pilot-reactor model that will be validated with the data obtained from the pilot plant reduction trials of different gas mixtures. The model will be capable of predicting residence time required for pellets reduced using variable gas mixtures consisting of CO and H_2. This way, it will be possible to show the effect of gradual transition or rapid shift from natural gas to hydrogen on the operation of the reactor shaft. Currently, a reactor with capacity to produce 1 ton per week of DRI is under construction for this purpose. Unlike the HYBRIT pilot plant[35] in Sweden which focuses on pure H_2, GISH pilot plant will explore much wider range of possible gas mixes for DRI pellets production. Thus, the industry will obtain a wide set of scenarios for risk-free transition from natural gas to hydrogen-reduction technologies.

2. Materials

The iron-ore (hematite) pellets for the study were supplied by Voestalpine AG, Texas, USA. Reaction gases H_2 gas of 99.99% purity used in TU Bergakademie Freiberg was supplied by Linde Gas. In Voestalpine Linz lab, H_2 and CO were also supplied by Linde Gas. A batch of commercial iron-ore hematite pellets for the experiments were supplied from the Voestalpine Texas (Midrex) plant. Same hematite ore pellets were used in all the experiments. Chemical composition of the pellets is given in **Table 1**.

A total of 250 randomly selected pellets were analyzed in our previous study[33] to document variations in their diameter by digital image analysis. The average diameter of the pellets was estimated as 13.54 ± 2.2 mm.

Unreacted pellets were analyzed using an apparent density method described later and their porosity was estimated to be $39 \pm 0.1\%$. However, pellets were found to have significant amounts of closed pores, as confirmed by the MIP method, which yielded only 28% porosity. As can be seen from the SEM–energy dispersive X-ray analysis (EDX) image in **Figure 3**, the shell of the pellet has higher porosity compared to the core. The pores in the core are larger and more isolated.

3. Experimental Section

Two different retorts were used for the reduction experiments. The one used in Voestalpine Linz lab had an inner diameter

Table 1. Samples chemical composition, mass %.

Fe_{tot}	FeO	Al_2O_3	CaO	SiO_2
67.8	0.35	0.49	0.76	1.34

© 2023 Wiley-VCH GmbH

1869344x, 0, Downloaded from https://onlinelibrary.wiley.com/doi/10.1002/srin.202300066 by Missouri University Of Science, Wiley Online Library on [16/08/2023]. See the Terms and Conditions (https://onlinelibrary.wiley.com/terms-and-conditions) on Wiley Online Library for rules of use; OA articles are governed by the applicable Creative Commons License

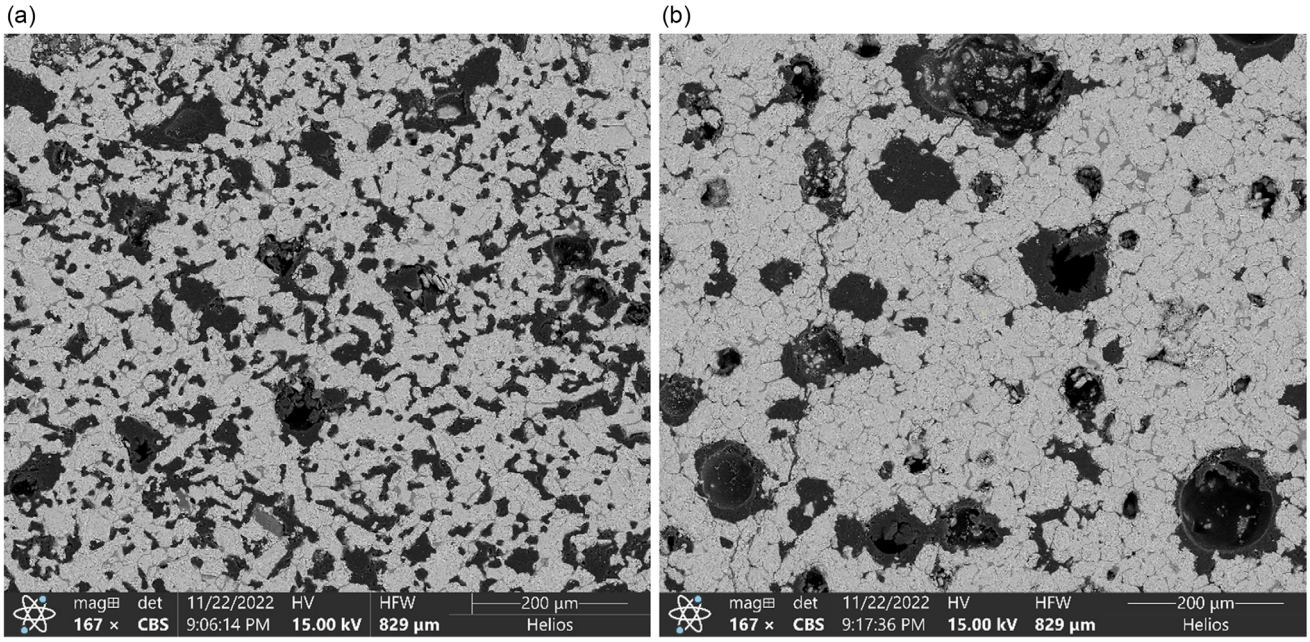

Figure 3. Scanning electron microscopy (SEM)–EDX image of unreacted pellet at ×167 magnification: a) the shell and b) the core of the pellet.

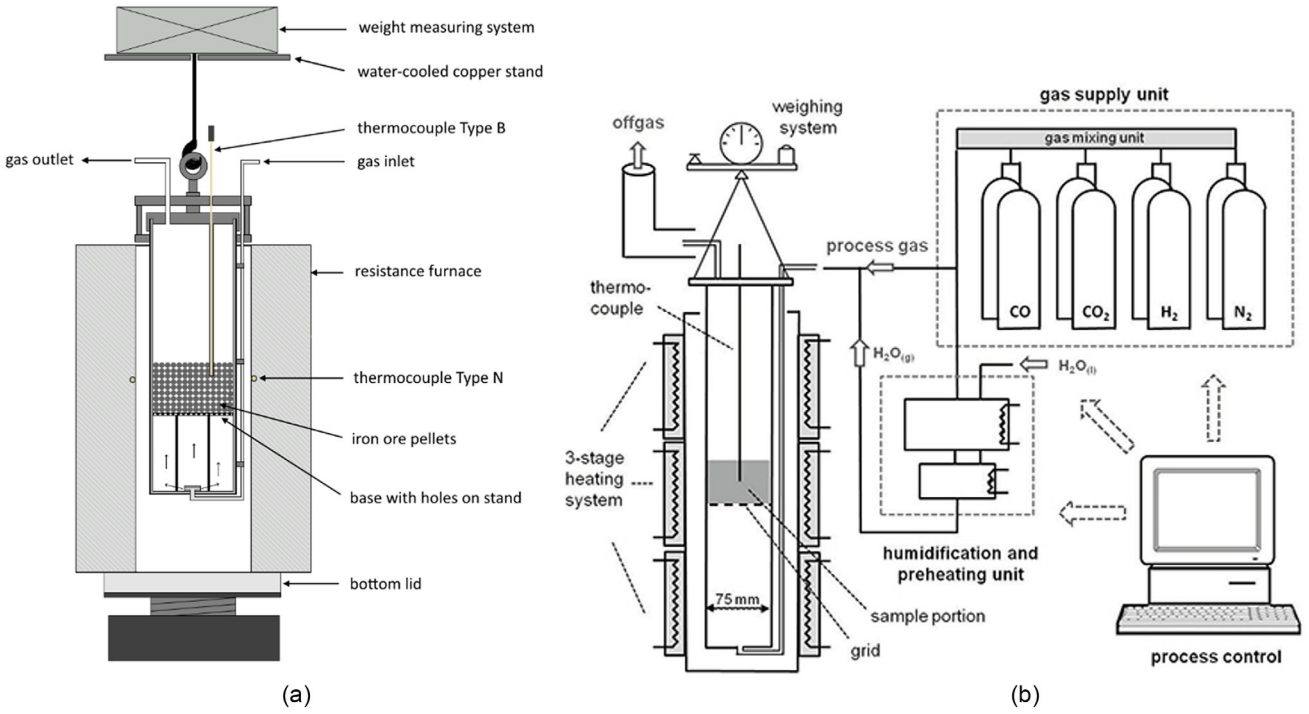

Figure 4. Scheme of the a) retort in the IIST laboratory , and b) retort furnace in Voestalpine laboratory.

of 75 mm (**Figure 4**b). The retort in the institute of iron and steel technology (IIST) lab had an inner diameter of 114 mm. Dimensions and scheme of the IIST lab are given in Figure 4a. The main purpose of the larger retort was to enable higher temperatures of reduction (which was not possible otherwise), and it could also give some insights on the effect of pellet bed size on H_2 reduction. The temperature of 900 °C for reduction was the maximum available for the existing equipment in IIST. Also, it was near the industrial practice of current MIDREX reactors.[36]

Experimental conditions in the two laboratories were different. The IIST lab retort was filled with 960–970 g of pellets,

© 2023 Wiley-VCH GmbH

1869344x, 0, Downloaded from https://onlinelibrary.wiley.com/doi/10.1002/srin.202300066 by Missouri University Of Science, Wiley Online Library on [16/08/2023]. See the Terms and Conditions (https://onlinelibrary.wiley.com/terms-and-conditions) on Wiley Online Library for rules of use; OA articles are governed by the applicable Creative Commons License

while the smaller retort in Voestalpine lab was filled with the 500 g. Gas flow rates and fraction of components in the gas mixtures were also different. Experiments in large retort were conducted at 12 L min^{-1} flow of pure H_2 (technical limit). Experiments in smaller retort were conducted at 50 L min^{-1} flow of gas mixtures as shown in **Table 2**. These gas mixtures simulated the industrial gas mixtures present in the reduction zone of the Midrex and HYL III reactors. Gas compositions were selected based on the industrial operation practices of GISH project partners—Voestalpine AG and Danieli SA who operated MIDREX and HYL III facilities, respectively. The hydrogen gas composition in the small retort simulated the assumed future industrial process of pure H_2 reduction of iron ores which utilized gas recycling. Therefore, H_2 mixture at the inlet in this experiment contained 8% of water vapor.

Retorts were heated to the target temperature with the argon gas supply and held for at least 20 min to reach an equilibrium temperature of the pellets bed. After this step, the reduction gas was initiated. Weight change was constantly recorded with the use of Mettler Toledo balance. After complete reduction, the reducing gas mixture was switched off and argon supply was started to cool the pellets in an inert atmosphere with an aim to prevent reoxidation of the freshly reduced iron. The weight of the cooled pellets was carefully measured.

To study the effects of various experimental parameters on the inner structure of the pellets, two classical methods were used—SEM and MIP.

Randomly selected pellets were embedded in epoxy and cut in half. After polishing with different mesh sandpaper and gold sputter coating, the samples were analyzed on the Helios 5 SEM machine.

Randomly selected pellets were also analyzed using the MIP method by the laboratory of Anton Paar with their Poremaster model porosimeter. This method allowed the open porosity of the samples to be quantified. The purpose of the MIP was to obtain a distribution of pore sizes. Measurement was performed at both low pressure (950–4.26 µm pore size) and high pressure (10.66–0.006 µm) modules of the porosimeter.

Apparent density of the pellets was measured as well to estimate the absolute pellet density (without porosity). A slightly modified procedure described previously in the paper of Monsen and Ringdalen was used.[37] Five randomly selected pellets were covered with superglue, which got absorbed in the pores and did not form thick layer on the surface of the pellet. Therefore, the volume change of the pellet due to the glue was neglected. The sealed pellets were held in a wire holder and then suspended in water. The amount of water displaced by the pellet in the holder was measured with the Sartorius balance with 0.0001 g resolution. Apparent density of the pellet was calculated using Formula (1)

$$\rho_{\text{app}} = \frac{m}{(V_{\text{t}} - V_{\text{s}})/\rho_{\text{w}}} \tag{1}$$

m—mass of pellet, V_{t}—volume of water displaced by the sample, V_{s}—volume of water displaced by the suspension, and ρ_{w}—density of water at room temperature.

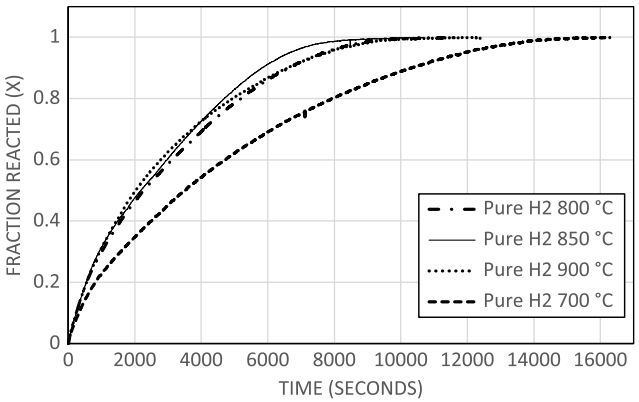

Figure 5. Conversion (X) of the 1 kg sample as a function of time at different temperatures.

Table 2. Conditions of experiments in the laboratories of Voestalpine and IIST.

Gas composition (excluding N_2 carrier gas)		Voestalpine			IIST			
		Midrex	HYL III	100% H_2	100% H_2			
H_2	[vol%]	56	75	92	100			
CO	[vol%]	36	18	0	–			
H_2O	[vol%]	6	3	8	–			
CO_2	[vol%]	2	4	0	–			
$(CO + H_2)/(CO_2 + H_2O)$	–	11.5	12.2	11.5	–			
Total gas flow	[L min^{-1}]	50	50	50	12			
N_2 gas flow	[L min^{-1}]	10	10	10	–			
Reducing gas flow	[L min^{-1}]	40	40	40	12			
Bed temperature	[°C]	850	850	850	700	800	850	900
Duration	[min]	180	180	180	270	200	200	200
Size of pellets	[mm]	–13.54	–13.54	–13.54	13.54	13.54	13.54	13.54
Sample size	[g]	500	500	500	980	980	980	980

© 2023 Wiley-VCH GmbH

1869344x, 0, Downloaded from https://onlinelibrary.wiley.com/doi/10.1002/srin.202300066 by Missouri University Of Science, Wiley Online Library on [16/08/2023]. See the Terms and Conditions (https://onlinelibrary.wiley.com/terms-and-conditions) on Wiley Online Library for rules of use; OA articles are governed by the applicable Creative Commons License

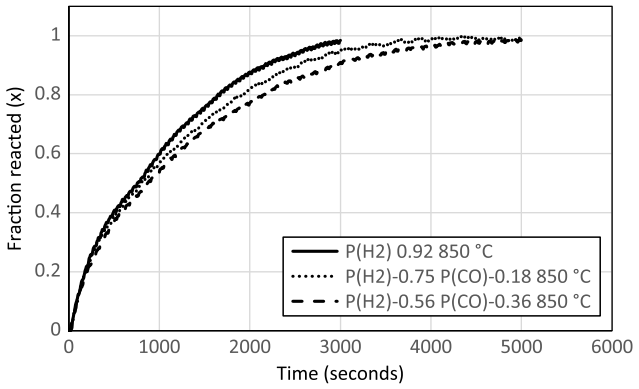

Figure 6. Conversion (X) of the 0.5 kg sample as a function of time at different gas compositions.

The density of the bulk pellet was calculated based on the chemical composition and bulk density for each individual chemical compound of pellet. For the unreacted pellets, the bulk density was estimated as 5.19 g cm^{-3}. Density of reduced pellets was calculated assuming 95% reduction at the time of measurement to account for possible reoxidation after the sample was taken from the cooling in argon atmosphere. Carbon content of the reduced pellets was measured using a LECO carbon combustion analyzer.

Table 3. Carbon content in the reduced pellets.

Sample	C [mass %]
700 H_2	0.011
800 H_2	0.021
850 H_2	0.009
900 H_2	0.014
Midrex	0.019
H_2	0.0097
HYL III	0.107

4. Results

The plots for the conversion (X) as a function of time (t) at different temperatures are shown in **Figure 5**. It can be seen from this plot that the X versus t curves at 800, 850, and 900 °C were close to each other. The fastest reduction occurred at 850 °C. In contrast, reduction at 700 °C took almost twice as long as at the other three temperatures. These curves complement the results and observations of Wagner et al.[21] who reported that temperature plays significant role on the reduction kinetics of iron-ore powder at temperatures below 800 °C. Compared to the 0.5 kg sample reduction time in Voestalpine lab (**Figure 6**), the reduction time of the 1 kg samples was nearly 3 times longer. We attribute this to the lower reduction strength in the gas for the latter case. The lower flow rate and larger bed size would result in a larger decrease in hydrogen concentration and more oxides left to reduce. The gas inside the retort was also mixed with the product of reaction—water vapor. For the case of the small retort, the ratio of reducing gases to reduction products ($H_2 + CO/H_2O + CO_2$) was higher than that of the big retort. Therefore, the reduction strength of the gas was considerably different in the two cases.

Increasing the fraction of CO in the H_2–CO gas mixture has been shown to slow down the rate of reduction.[30,31,38] It is well known that H_2 has a higher-gas-phase-diffusion rate due to its smaller molecule size compared to CO gas.[11,14,21,39] For example, at the temperature of 850 °C, self-diffusion coefficients of H_2 and CO are 1.31×10^{-3} and 1.95×10^{-4} $m^2 s^{-1}$, respectively, at 1 atmosphere (based on own calculations).

As shown in **Table 3**, very little carbon deposition was observed in all the experiments except for a slight increase of carbon content for HYL III gas mixture. The same results of no-carbon deposition for reduction in various CO–H_2 gas mixtures and similar temperatures were reported by Barde et al.[22] The small amounts of C measured in the H_2-reduced pellets in this study may be sourced from initial unreacted pellet content.

Results of open porosity measurements were considerably different in the series with temperature variation. After reduction, the pellets showed a range of porosities between 46% and 74%

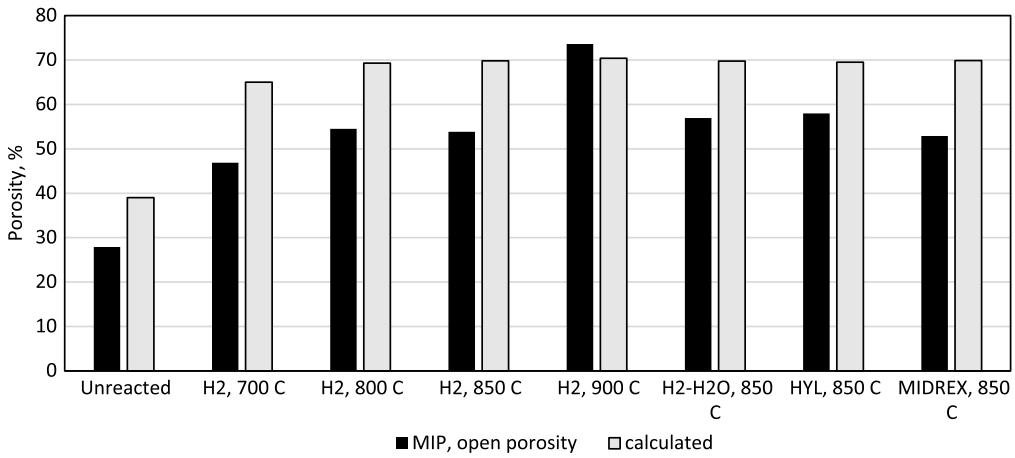

Figure 7. Porosity of the pellets measured with the mercury intrusion porosimeter and calculated based on apparent density measurements.

© 2023 Wiley-VCH GmbH

1869344x, 0, Downloaded from https://onlinelibrary.wiley.com/doi/10.1002/srin.202300066 by Missouri University Of Science, Wiley Online Library on [16/08/2023]. See the Terms and Conditions (https://onlinelibrary.wiley.com/terms-and-conditions) on Wiley Online Library for rules of use; OA articles are governed by the applicable Creative Commons License

(**Figure 7**). A slight increase in porosity was observed with reduction temperature in the present work, which complements the observations of Abdelrahim et al.[40] where porosity increased up to 1100 °C. However, the specific surface area in that study was observed to decrease with temperature.[40] The same result was reported previously in other sources.[41,42] This suggests that sintering is occurring only locally at the scale of newly formed metal whiskers, and it is not affecting macroscale pores. In recent work of Scharm et al.,[42] porosity was also reported to increase with temperature. On the contrary, El-Geassy and Nasr[17] observed a decrease of porosity of H_2-reduced hematite compacts which were similar to the initial porosity of 35% of pellets observed in this study.

MIP confirmed that the pore size distribution of the samples changed with both temperature and reducing gas composition (**Figures 8** and **9**). According to the MIP measurements, the smallest pores were obtained for reduction at 700 °C and the largest pores were found in samples reduced at 900 °C. In the present work, pores obtained for a H_2–CO–H_2O- (Midrex and HYL III) reducing gas mixtures were coarser than pores obtained for a H_2–H_2O mixture (e.g., compare the respective lines in Figure 8). These results confirm the conclusions of Turkdogan et al.[31,41] who reported coarser pores for higher reduction temperatures and for higher fraction of CO compared to a pure H_2-reducing gas mixture. They also complement the results of Abdelrahim et al.[40] who observed the formation of smaller pores

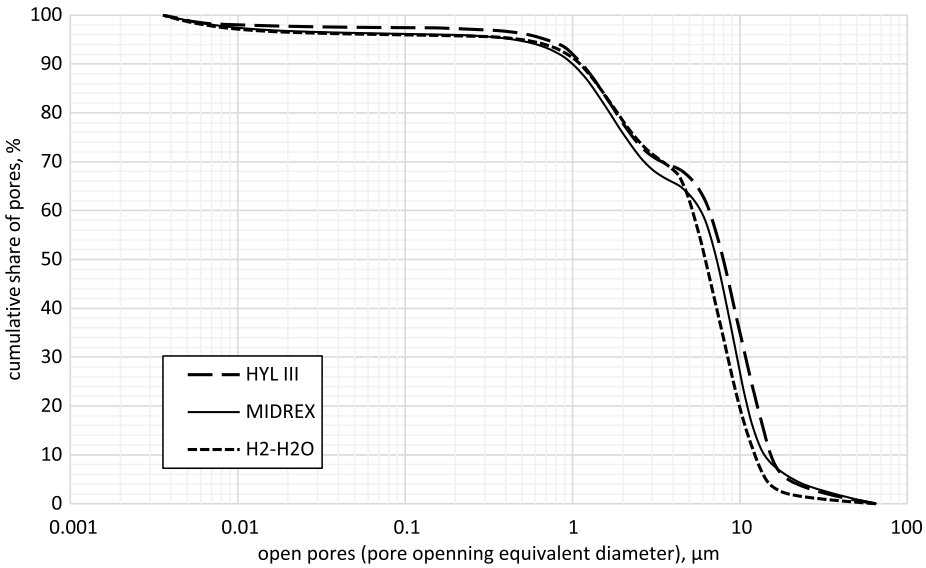

Figure 8. Pore size distribution as a function of the reduction gas mixture at temperature 850 °C in small retort.

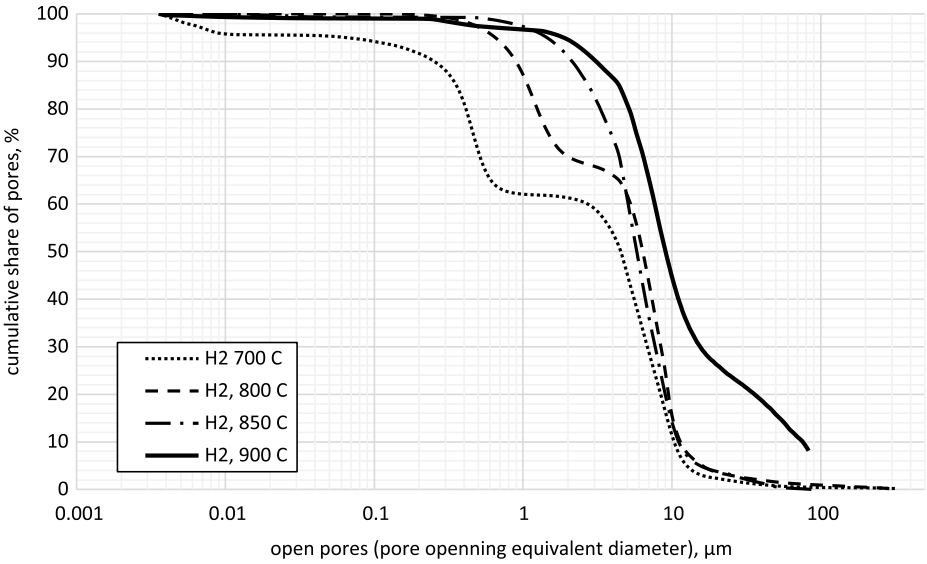

Figure 9. Pore size distribution as a function of temperature for large retort test.

© 2023 Wiley-VCH GmbH

1869344x, 0, Downloaded from https://onlinelibrary.wiley.com/doi/10.1002/srin.202300066 by Missouri University Of Science, Wiley Online Library on [16/08/2023]. See the Terms and Conditions (https://onlinelibrary.wiley.com/terms-and-conditions) on Wiley Online Library for rules of use; OA articles are governed by the applicable Creative Commons License

at 700 °C and higher H_2 content in the gas mixture. Another interesting observation in present work is that there is a significant discrepancy between porosity measured with two different methods. Most likely this discrepancy arises since MIP is capable of infiltrating only the open pores, while the absolute density measurement is able to account for the closed pores as well. Results show that the unreacted pellet had a large number of closed pores. The same is true for the reduced pellets except for the 900 °C test, where most of the pores tend to be open. Open porosity data for that particular sample was higher than the average total porosity measured for the other 5 samples reduced
at 900 °C.

The pellet structures varied with temperature. The pellet reduced at 700 °C (**Figure 10**) has a structure resembling relatively large densely packed coarse particles. These coarse particles have many very fine micropores. There is however no clear network of macropores. An increase in reduction

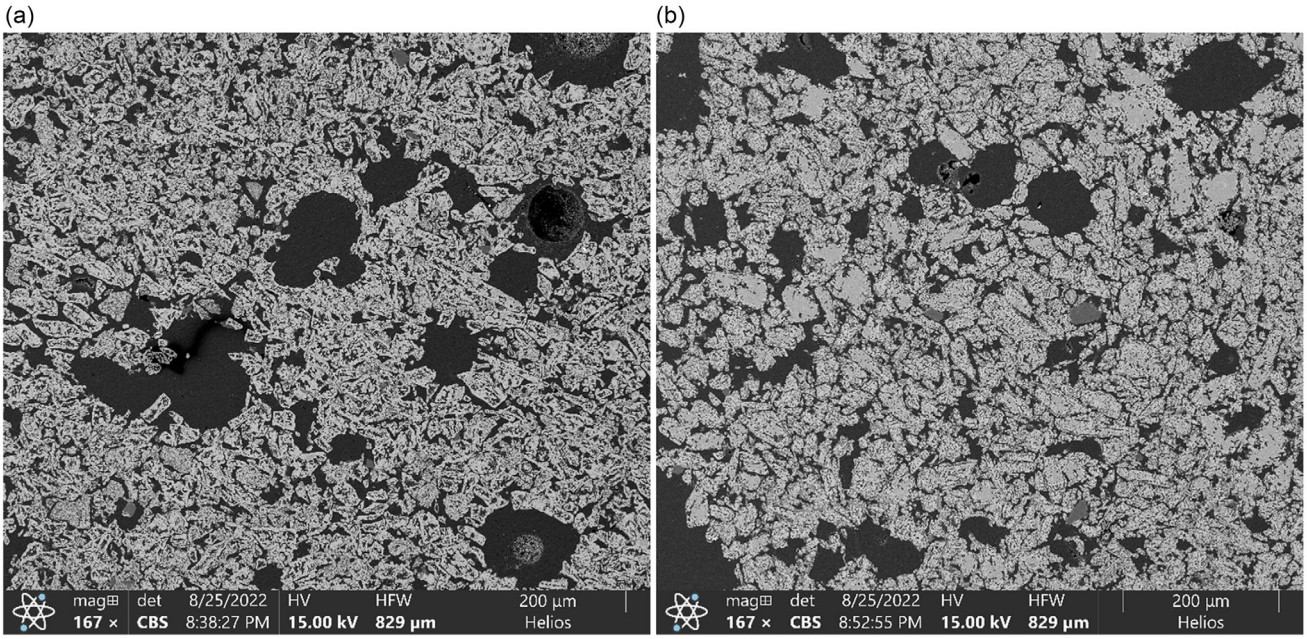

Figure 10. SEM images of the polished sample reduced with H_2 at 700 °C: a) shell and b) core.

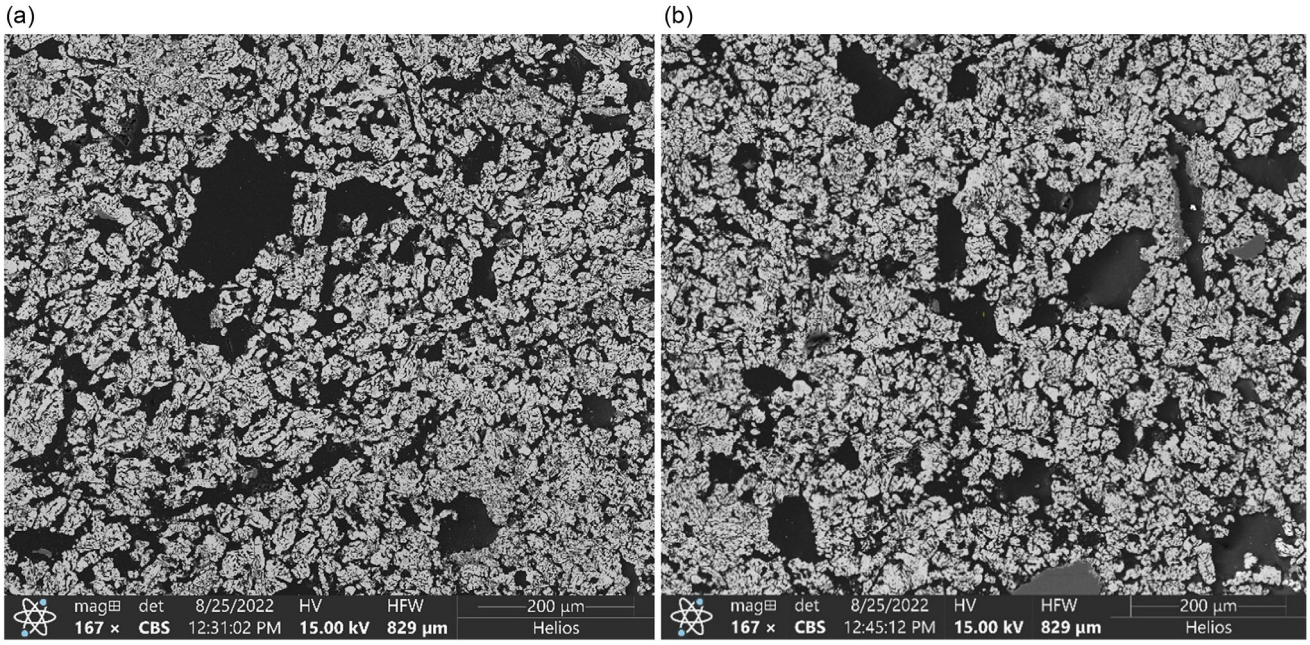

Figure 11. SEM images of the polished sample reduced with H_2 at 800 °C: a) shell and b) core.

 © 2023 Wiley-VCH GmbH

1869344x, 0, Downloaded from https://onlinelibrary.wiley.com/doi/10.1002/srin.202300066 by Missouri University Of Science, Wiley Online Library on [16/08/2023]. See the Terms and Conditions (https://onlinelibrary.wiley.com/terms-and-conditions) on Wiley Online Library for rules of use; OA articles are governed by the applicable Creative Commons License

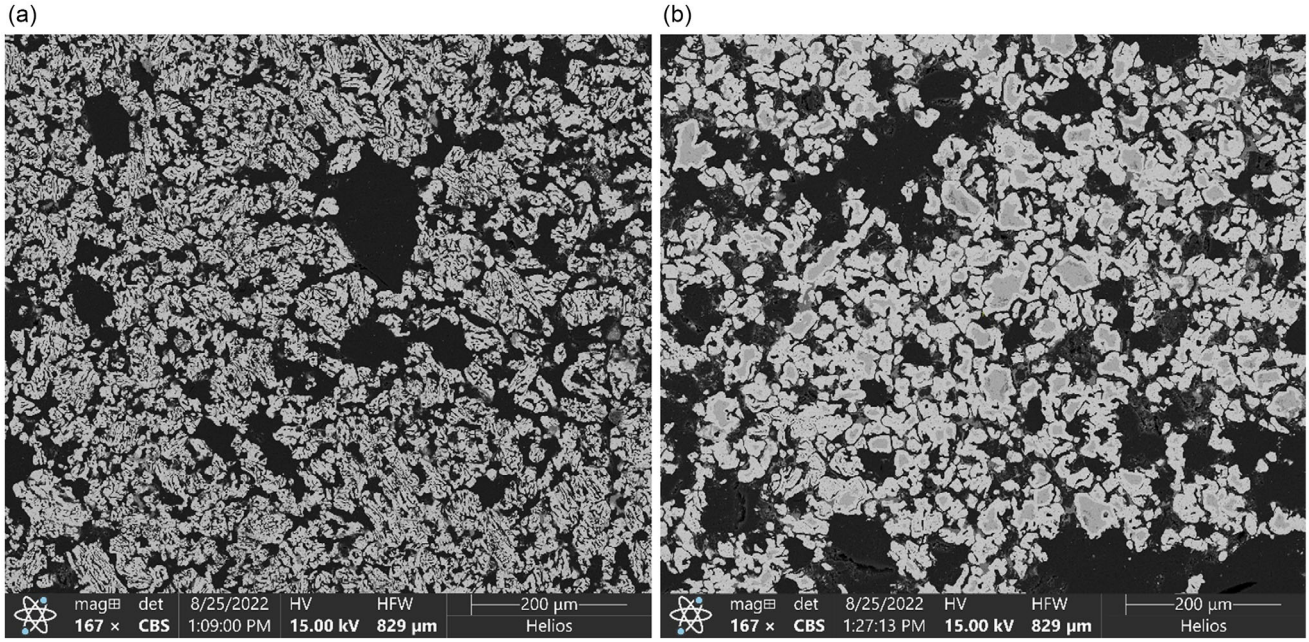

Figure 12. SEM images of the polished sample reduced with H_2 at 850 °C: a) shell and b) core.

temperature to 800 °C (**Figure 11**) resulted in fewer coarser grains and a more developed macropore network. A slight increase of reduction temperature to 850 °C (**Figure 12**) led to dramatic difference of the internal structure of the pellet. The shell part of the pellet retained nearly the same structure as the 800 °C sample. But the core of the pellet displayed very well sintered smooth grains with a well-developed macropores network and almost a negligible amount of micropores. Further growth of reduction temperature to 900 °C (**Figure 13**), however, yielded a structure with a well-developed macropore network while some micropores still remaining in both core and shell. These results indicate that the sintering and agglomeration process of grains in core region could have been more significant at 850 °C than at 900 °C. Similar trend was also observed by Turkdogan et al.[41] In their work, total porosity of hematite particles reduced using H_2 was observed to increase from 600 °C up

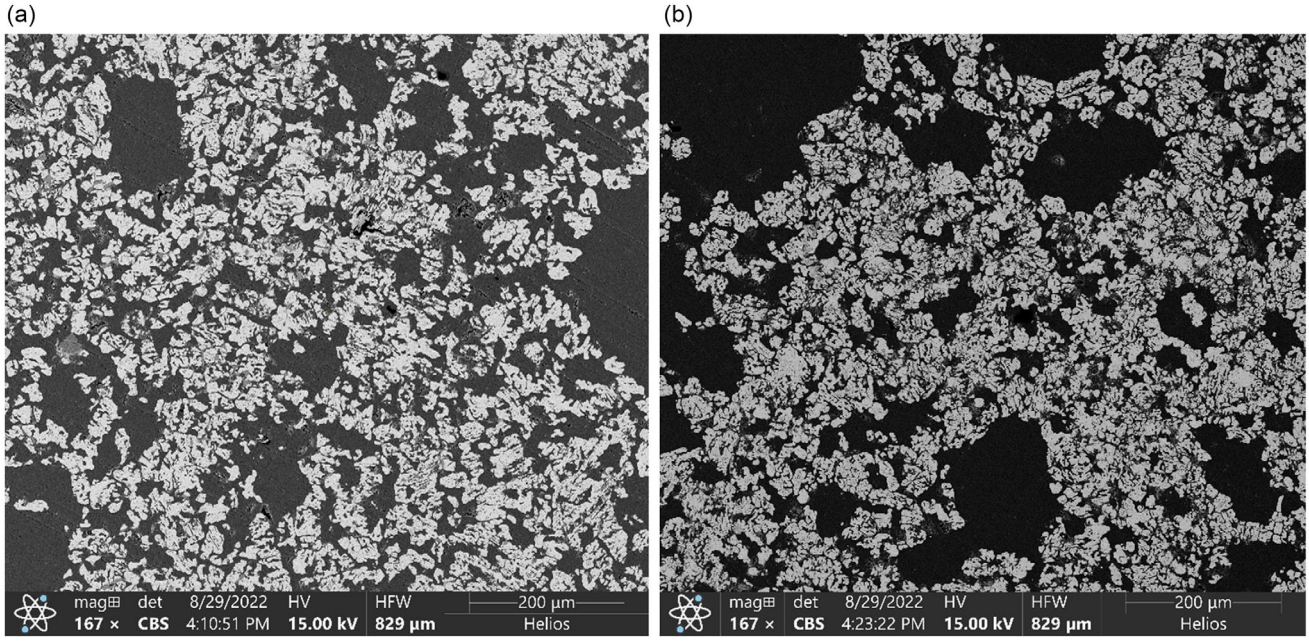

Figure 13. SEM images of the polished sample reduced with H_2 at 900 °C: a) shell and b) core.

© 2023 Wiley-VCH GmbH

1869344x, 0, Downloaded from https://onlinelibrary.wiley.com/doi/10.1002/srin.202300066 by Missouri University Of Science, Wiley Online Library on [16/08/2023]. See the Terms and Conditions (https://onlinelibrary.wiley.com/terms-and-conditions) on Wiley Online Library for rules of use; OA articles are governed by the applicable Creative Commons License

to the temperature of 800 °C where the maximum was reached. At higher temperatures, the porosity decreased (900 °C) but increased at 1000 °C and finally decreased by 1100 °C, and 1100 °C was the temperature when most likely the sintering process manifests. Scharm et al.[42] also reported abnormal drop of porosity at 900 °C in H_2-reduced pellets. This decrease in the porosity may indicate sintering and recrystallization in the temperature interval between 800 and 900 °C at low reduction rates which can be specific to the ore type. Observed sintering at 850 °C may be the main explanation why reduction rate was very close for 800, 850, and 900 °C.

The samples, from the reduction experiments carried out in the Linz Laboratory, which exhibited the shortest reduction time with the H_2–H_2O mixture (**Figure 14**), had a very fine pore network inside the pellet's grains. The sample reduced with an HYL III gas mixture (**Figure 15**) had less micropores and a well-developed network of macropores. The MIDREX gas composition (**Figure 16**) led to the slowest reduction rate among the small

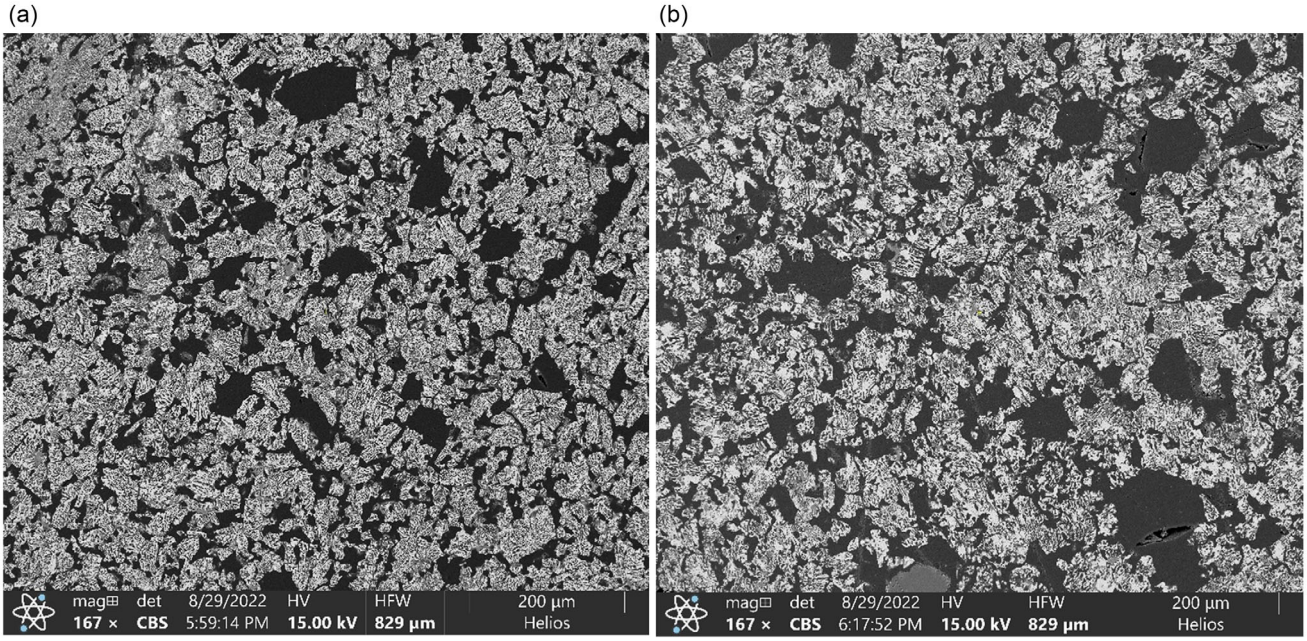

Figure 14. SEM image of H_2–H_2O gas-mix-reduced sample reduced at 850 °C: a) shell and b) core.

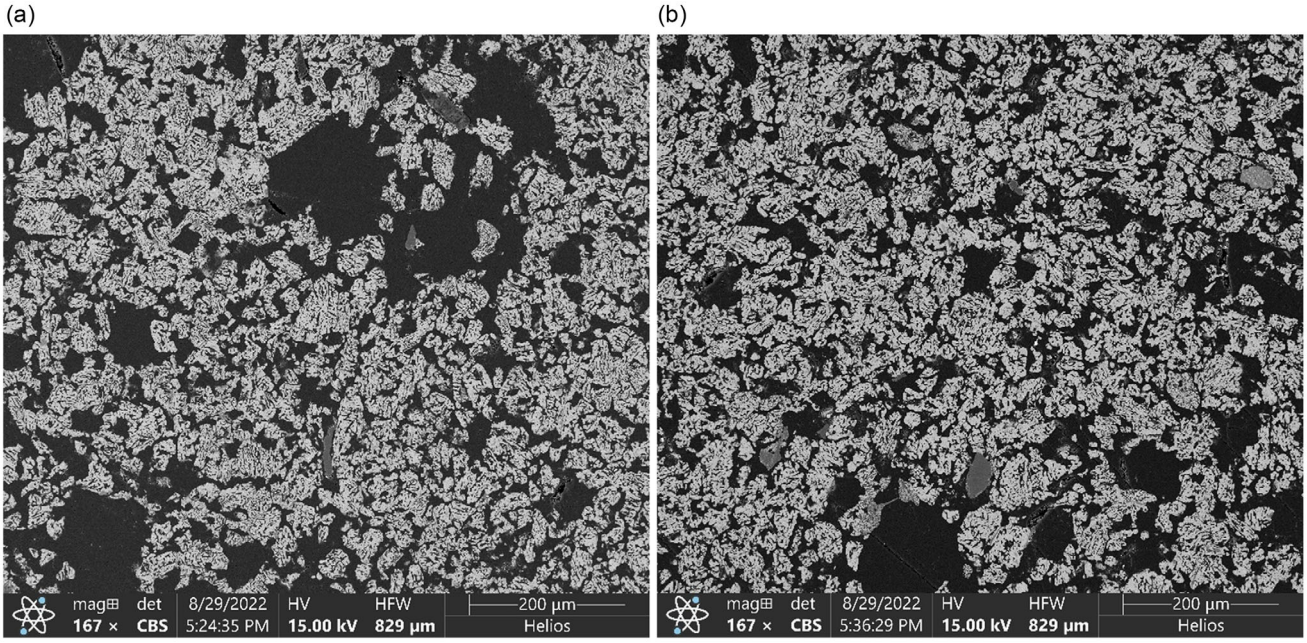

Figure 15. SEM image of HYL-III-simulated gas mixture sample reduced at 850 °C: a) shell and b) core.

© 2023 Wiley-VCH GmbH

1869344x, 0, Downloaded from https://onlinelibrary.wiley.com/doi/10.1002/srin.202300066 by Missouri University Of Science, Wiley Online Library on [16/08/2023]. See the Terms and Conditions (https://onlinelibrary.wiley.com/terms-and-conditions) on Wiley Online Library for rules of use; OA articles are governed by the applicable Creative Commons License

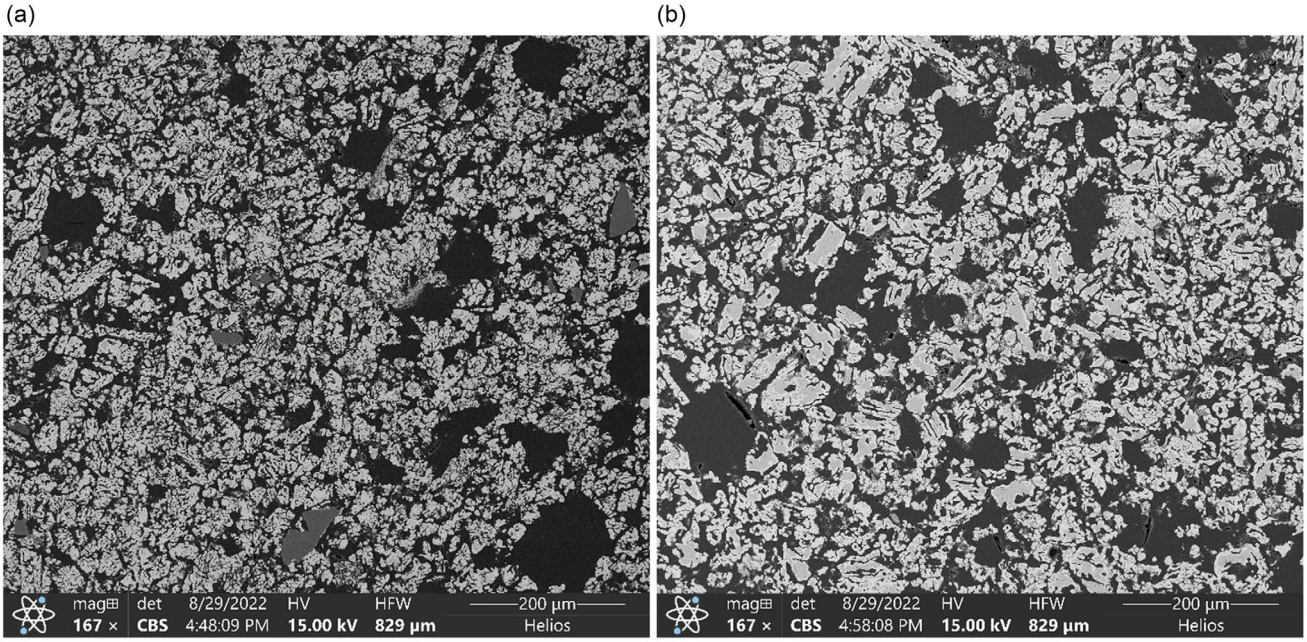

Figure 16. SEM image of MIDREX-simulated gas mixture sample reduced at 850 °C: a) shell and b) core.

retort series, and the internal structure of the pellet somewhat resembles the features of the pure H_2-reduced pellet as shown in Figure 9 reduced in the big retort at much slower rate. Taking into account that reduction times in the small retort were at least half as long as reduction times in a big retort, the difference in structure of pellets obtained at 850 °C in IIST and Linz can be explained by the longer time at temperature for sintering of metallic Fe grains in the larger retort.

Overall, the pore surface area in the iron product layer has a positive but not a linear effect on the reduction rate. The reason is that most of the reduction happens on the surface of large interconnected pores instead of small pores.[31] The formation of finer pores, when not associated with growing of interconnected channels, should lead to less effective diffusion of gas, which reduces the overall positive effect of the higher pore surface area on the reduction rate.

It is notable that reduction with pure H_2 at lower gas flow rates in the 1 kg retort led to formation of the much coarser pores compared to H_2 reduction and even compared to HYL III and MIDREX gas mixes in 0.5 kg retort. This suggests that reduction rate has more effect on the porosity than the type of gas used. Previously, Turkdogan and Winters[31] have suggested that a slower reduction rate is the main cause of the coarser pores for CO compared to H_2. In the present research, we were able to confirm this hypothesis with both SEM and MIP analysis. This potential role of reduction rate on porosity could have a

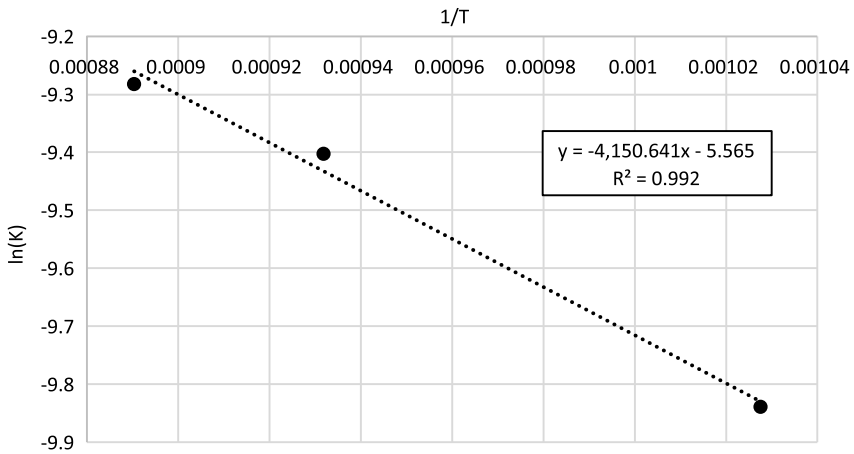

Figure 17. Reaction rate constant K as a function of temperature.

© 2023 Wiley-VCH GmbH

1869344x, 0, Downloaded from https://onlinelibrary.wiley.com/doi/10.1002/srin.202300066 by Missouri University Of Science, Wiley Online Library on [16/08/2023]. See the Terms and Conditions (https://onlinelibrary.wiley.com/terms-and-conditions) on Wiley Online Library for rules of use; OA articles are governed by the applicable Creative Commons License

significant impact on product quality of DRI. The porosity of the pellets affects their structural strength[43] and potentially the subsequent melting behavior of DRI.

5. Activation Energy

The rate constants $k(T)$ for the pure H_2 experiments performed at 700, 800, and 850 °C was determined by fitting the experimental data of the contracting sphere model. The equation for the contracting sphere model is given as follows[11]

$$k(T) \times t = g(X) = 1 - (1 - X)^{1/3} \tag{2}$$

The slope of $g(X)$ versus t curve was then used to determine $k(T)$ for each experiment. A plot of $\ln(k(T))$ versus $1/T$ was obtained (**Figure 17**) and the resulting slope of the best fitting line was used in the Arrhenius equation to determine the activation energy, as shown in the following[44]

$$E_a = -R\frac{d\ln k(T)}{d(1/T)} \tag{3}$$

From the calculations, the activation energy was found to be 34.50 KJ mol^{-1} which is in the range of previously reported in literature.[11] It has been reported that the activation energy range is 4.2–21 KJ mol^{-1} when the rate limiting step is internal diffusion and over 42 kJ mol^{-1} is interfacial chemical reaction.[45] Our value of activation energy for pure hydrogen reduction falls in between internal diffusion and chemical reaction resistance cases (**Table 4**).

Table 4. Parameters of reduction reactions as given on Figure 16.

T [°C]	$k(T)$	T [K]	1 T^{-1}	ln(K)
700	0.00005333	973.15	0.001027591	−9.83901
800	0.00008256	1073.15	0.000931836	−9.40199
850	0.00009314	1123.15	0.000890353	−9.28141

An approximate analysis of the rate controlling step was done using the analytical calculations and equations of the shrinking core model reported by Zuo, Hai-bin et al.[30] In short, these analytical calculations solved of the shrinking core model - Equation (4) - which considers all three resistances: film diffusion resistance, ash diffusion (reacted shell) resistance, and chemical reaction resistance to give an approximate value for effective diffusion coefficient and the reaction rate constant.

$$V_t = \frac{4\pi r_0^2(C_b - C_e)}{\frac{1}{k_g} + \frac{r_0(r_0 - r_i)}{D_{eff}\, r_i} + \frac{K^\theta}{k_{rec}(1+K^\theta)\left(\frac{r_0}{r_i}\right)^2}} \tag{4}$$

Here, V_t is the rate of reaction [mol s^{-1}]; r_0 is the initial radius of the pellet [m]; C_b is the concentration of reactant gas [mol m^{-3}]; C_e is the equilibrium concentration of the reactant gas [mol m^{-3}]; r_i is the radius of the unreacted core of the pellet [m]; k_g is the mass transfer diffusion coefficient in the gas film, [m s^{-1}]; D_{eff} is the effective diffusion coefficient of gaseous species [m^2 s^{-1}]; k_{rec} is the reaction rate constant [m s^{-1}]; and K^θ is the equilibrium constant of chemical reaction.

Further, Zuo et al.[30] transformed this equation using four parameters C_1, C_2, F, and t_1 to obtain a linear plot (**Figure 18**) and extract the values of effective diffusion coefficient (D_{eff}) and reaction rate constant (k_{rec}) using the slope (C_1) and the y-intercept (C_2), respectively. The mass transfer coefficient (k_g) was calculated using its relationship between Reynold's number, Schmidt number and the diffusion coefficient.

$$\frac{t - t_1}{F} = C_1(3F - 2F^2) + C_2 \tag{5}$$

$$C_1 = \frac{r_0^2 d_0}{6D_{eff}(C_b - C_e)} \tag{6}$$

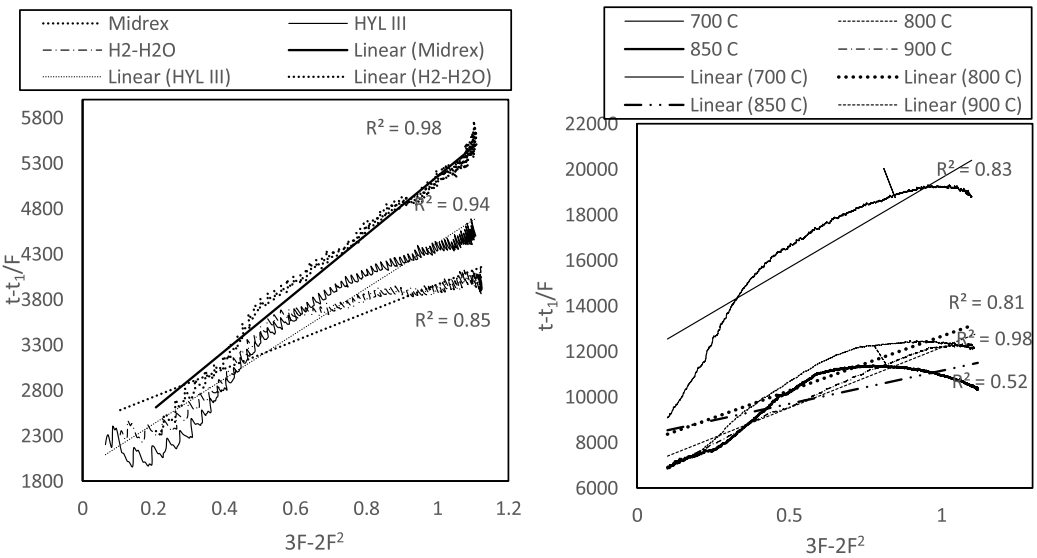

Figure 18. Curves for mixed control model obtained from reduction versus time data.

© 2023 Wiley-VCH GmbH

1869344x, 0, Downloaded from https://onlinelibrary.wiley.com/doi/10.1002/srin.202300066 by Missouri University Of Science, Wiley Online Library on [16/08/2023]. See the Terms and Conditions (https://onlinelibrary.wiley.com/terms-and-conditions) on Wiley Online Library for rules of use; OA articles are governed by the applicable Creative Commons License

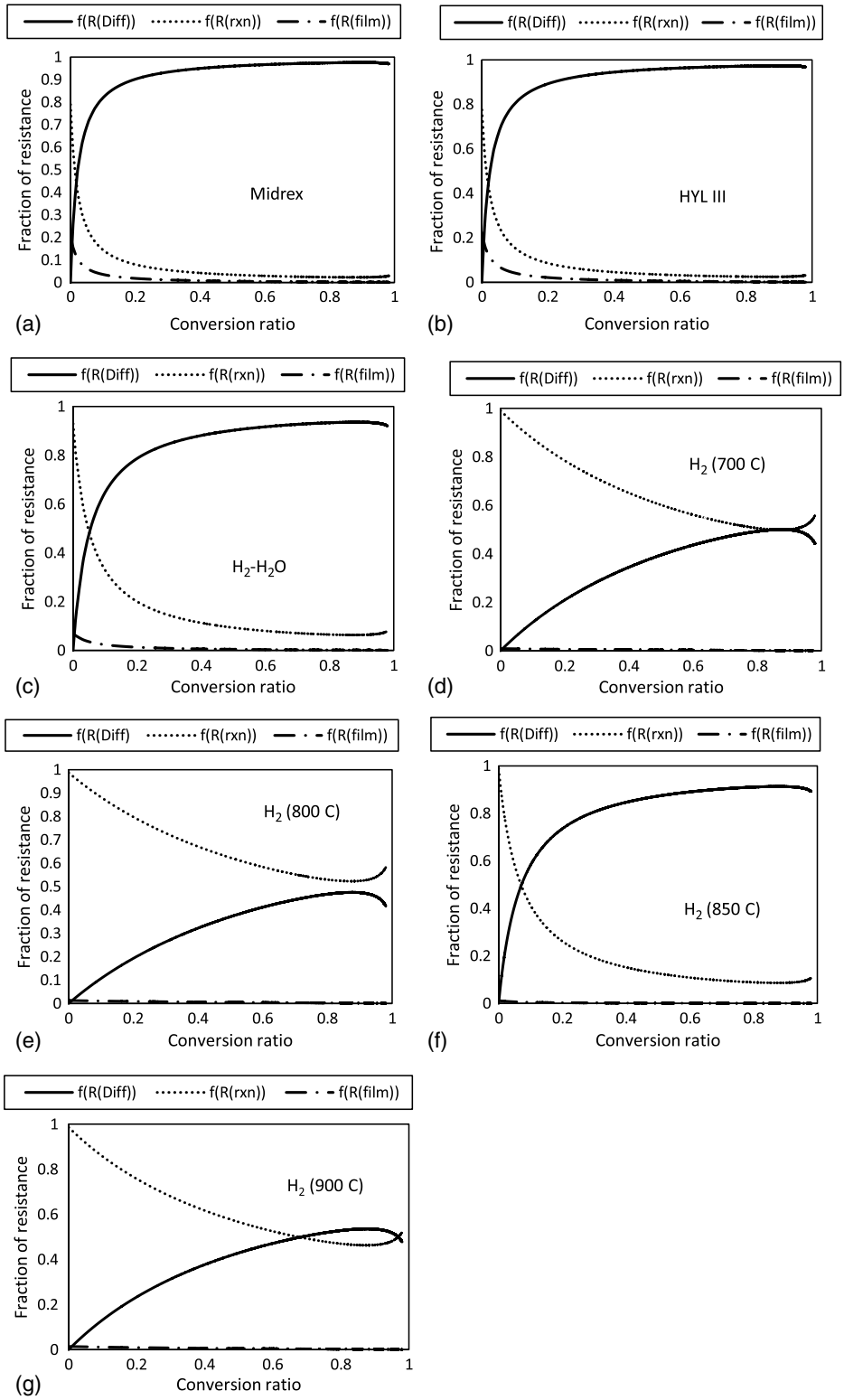

Figure 19. a–g) Fraction of relative resistances of as a function of conversion.

© 2023 Wiley-VCH GmbH

1869344x, 0, Downloaded from https://onlinelibrary.wiley.com/doi/10.1002/srin.202300066 by Missouri University Of Science, Wiley Online Library on [16/08/2023]. See the Terms and Conditions (https://onlinelibrary.wiley.com/terms-and-conditions) on Wiley Online Library for rules of use; OA articles are governed by the applicable Creative Commons License

$$C_2 = \frac{K^{\theta} r_0 d_0}{k_{\mathrm{rec}}(1 + K^{\theta})(C_{\mathrm{b}} - C_{\mathrm{e}})} \tag{7}$$

$$F = 1 - (1 - X)^{\frac{1}{3}} \tag{8}$$

$$t_1 = \frac{r_0 d_0 X}{3k_{\mathrm{g}}(C_{\mathrm{b}} - C_{\mathrm{e}})} \tag{9}$$

Here, d_0 is the oxygen density of the pellet [mol m^{-3}] and t is the time [s]. It is evident that linear fit used in Zuo[30] model works better for the cases of mix gas (where R^2 values are well above 0.9) than for pure hydrogen where the R^2 value is in the range of 0.5–0.85. R^2 value was high only in one H_2 reduction case—at 900 °C.

As can be seen in **Figure 19**, chemical reaction resistance was dominating for most of the time of reduction with H_2 at 700, 800, and 900 °C in the big retort test (Figure 19d–g) where the gas flow rate was relatively low. Reaction resistance was also dominating in the beginning of reduction (5%–10% of conversion) in the 850 °C. However, after initial reduction, phase diffusion resistance becomes dominant. It is interesting that resistances in big retort at 850 °C (Figure 19f) repeat the same pattern as those in the small retort (Figure 19c) exhibiting diffusion resistance dominance. For the tests at other temperatures (both lower and higher) in the big retort, reaction resistance was the major contributor to the overall resistance. This is somewhat puzzling but the results could point at potential sintering occurring at 850 °C causing diffusion to become slower. When examining Figure 12b, the smaller pores are absent in the core when compared to Figures 11b and 13b. As for the mixed gas experiments, diffusion control could be attributed to the smaller pore size evident in Figures 8 and 14–16. The model suggests that gas-film resistance plays noticeable role only in the initial stage of mixed-gas reduction test, while in the H_2 tests conducted, its role can be neglected.

6. Conclusions

A series of reduction experiments with iron-ore pellets using various gas mixtures and temperatures were performed. The kinetics of the reduction and porosity of the reduced pellets were measured: 1) An increase in temperature from 700 to 800 °C led to considerably faster (almost 2 times faster) reduction in pure H_2 atmosphere. A further increase to 900 °C improved reduction kinetics only marginally. 2) The total porosity of the fully reduced samples is between 69% and 71% of volume for all conditions except for reduction at 700 °C, which had approximately 64% porosity. The open porosity measured by MIP was lower than total porosity measured by immersion method and varied much more indicating effect of temperature on the ratio of open and closed pores. 3) Pore size distribution of reduced pellets varied with temperatures and gas mix. The smallest pores were obtained for reduction at the lowest temperature in test series and for the H_2/H_2O gas mixture in the gas mix series. 4) A lower gas flow rate and corresponding lower reduction rate yielded much coarser pores in the reduced pellets indicating the stronger local sintering of particles or iron whiskers at low reduction rates. The effect of reduction rate on the porosity of the iron pellets in present study clearly offsets the effect of gas composition. 5) The main kinetic resistance for reduction at the gas flow rates employed at 850 °C is gas diffusion, while for the 700 and 800 °C chemical reaction dominated the resistance. Gas-film resistance played only a minor role at the initial stages of reduction.

The results of present work are being employed in the development of a numerical model of the iron-ore pellet reduction process under various gas and temperatures in the reactor shaft for the GISH project. Additional work is also being performed with individual pellets to evaluate reduction kinetics for various gas atmospheres and temperatures.

Acknowledgements

This material is based upon work supported by the U.S. Department of Energy's Office of Energy Efficiency and Renewable Energy (EERE) under the Hydrogen and Fuel Cell Technologies Office (Grant no. DE-EE0009250). Authors would like to acknowledge also the help of Peter Neuhold, Dr. Hans-Peter Heller, Fred Pena, and David Write in preparing the experiments, as well as Michelle Herrera for helping with chemical analysis. The assistance of all of our GISH project industry supporters (Nucor, SDI, Voestalpine, Gerdau, ArcelorMittal, Linde, Praxair, and Danieli) is also gratefully acknowledged. The authors also acknowledge the use of facilities within the Eyring Materials Center at Arizona State University.

Conflict of Interest

The authors declare no conflict of interest.

Full Legal Disclaimer

This report was prepared as an account of work sponsored by an agency of the United States Government. Neither the United States Government nor any agency thereof, nor any of their employees, makes any warranty, express or implied, or assumes any legal liability or responsibility for the accuracy, completeness, or usefulness of any information, apparatus, product, or process disclosed, or represents that its use would not infringe privately owned rights. Reference herein to any specific commercial product, process, or service by trade name, trademark, manufacturer, or otherwise does not necessarily constitute or imply its endorsement, recommendation, or favoring by the United States Government or any agency thereof. The views and opinions of authors expressed herein do not necessarily state or reflect those of the United States Government or any agency thereof.

Abridged Legal Disclaimer

The views expressed herein do not necessarily represent the views of the U.S. Department of Energy or the United States Government.

Data Availability Statement

The data that support the findings of this study are available on request from the corresponding author. The data are not publicly available due to privacy or ethical restrictions.

© 2023 Wiley-VCH GmbH

1869344x, 0, Downloaded from https://onlinelibrary.wiley.com/doi/10.1002/srin.202300066 by Missouri University Of Science, Wiley Online Library on [16/08/2023]. See the Terms and Conditions (https://onlinelibrary.wiley.com/terms-and-conditions) on Wiley Online Library for rules of use; OA articles are governed by the applicable Creative Commons License

Keywords

CO, direct reduction, hematite, hydrogen, iron ores, pellets, porosity

Received: February 4, 2023
Revised: April 24, 2023
Published online:

[1] *Iron and Steel Technology Roadmap - Towards More Sustainable Steelmaking*, IEA, Paris, France **2020**.
[2] S. Santos, *Iron and Steel CCS Study (Techno-Economics Integrated Steel Mill)*, IEAGHG, Cheltenham, UK **2013**.
[3] F. Memoli, *AIST* **2022**, *2022*.
[4] J. Cappel, F. Ahrenhold, M. W. Egger, H. Hiebler, J. Schenk, *Metals* **2022**, *12*, 912.
[5] J. C. Agarwal, F. C. Brown, D. L. Chin, G. S. Stevens, D. M. Smith, *Fuel Energy Abstr.* **2000**, *41*, 404.
[6] V. Chevrier, *presented at the Sustainable Energy Economy Workshop*, Toledo, OH, January 2020.
[7] Energiron technology, https://www.energiron.com/technology/ (accessed: April 2023).
[8] International Energy Agency, *Global Hydrogen Review 2021*, OECD, Paris, France **2021**, https://doi.org/10.1787/39351842-en.
[9] D. Pauluzzi, A. Hertrich Giraldo, A. Zugliano, D. Dalle Nogare, A. Martinis, in *AISTech2020 Proc. of the Iron and Steel Technology Conf.*, AIST, Cleveland, OH, August–September **2021**, https://doi.org/10.33313/380/056.
[10] H. J. T. Ellingham, *J. Soc. Chem. Ind.* **1944**, *63*, 125.
[11] D. Spreitzer, J. Schenk, *Steel Res. Int.* **2019**, *90*, 1900108.
[12] F. Patisson, O. Mirgaux, *Metals* **2020**, *10*, 922.
[13] A. Heidari, N. Niknahad, M. Iljana, T. Fabritius, *Materials* **2021**, *14*, 7540.
[14] A. Zare Ghadi, M. S. Valipour, S. M. Vahedi, H. Y. Sohn, *Steel Res. Int.* **2020**, *91*, 1900270.
[15] L. von Bogdandy, H.-J. Engell, *The Reduction of Iron Ores*, Springer Berlin Heidelberg, Berlin, Heidelberg **1971**, https://doi.org/10.1007/978-3-662-10400-2.
[16] M. Bahgat, M. H. Khedr, *Mater. Sci. Eng. B* **2007**, *138*, 251.
[17] A. A. El-Geassy, M. I. Nasr, *Trans. ISIJ* **1988**, *28*, 650.
[18] S. K. El-Rahaiby, Y. K. Rao, *Metall. Trans. B* **1979**, *10*, 257.
[19] H. Chen, Z. Zheng, Z. Chen, X. T. Bi, *Powder Technol.* **2017**, *316*, 410.
[20] O. A. Teplov, *Russ. Metall. Met.* **2012**, *2012*, 8.
[21] D. Wagner, O. Devisme, F. Patisson, D. Ablitzer, in *Proc. of the 2006 TMS Fall Extraction and Processing Division: Sohn Int. Symp.*, San Diego, August 2006.
[22] A. A. Barde, J. F. Klausner, R. Mei, *Int. J. Hydrog. Energy* **2016**, *41*, 10103.
[23] M.-H. Bai, H. Long, S.-B. Ren, D. Liu, C.-F. Zhao, *ISIJ Int.* **2018**, *58*, 1034.
[24] M. N. Abu Tahari, F. Salleh, T. S. Tengku Saharuddin, A. Samsuri, S. Samidin, M. A. Yarmo, *Int. J. Hydrogen Energy* **2021**, *46*, 24791.
[25] M. Kazemi, M. S. Pour, D. Sichen, *Metall. Mater. Trans. B* **2017**, *48*, 1114.
[26] A. A. El-Geassy, V. Rajakumar, *Trans. ISIJ* **1985**, *25*, 1202.
[27] A. Bonalde, A. Henriquez, M. Manrique, *ISIJ Int.* **2005**, *45*, 1255.
[28] E. A. Mousa, A. Babich, D. Senk, *Steel Res. Int.* **2013**, *84*, 1085.
[29] P. Cavaliere, A. Perrone, D. Marsano, V. Primavera, *Steel Res. Int.* **2023**, *94*, 2200791.
[30] H. Zuo, C. Wang, J. Dong, K. Jiao, R. Xu, *Int. J. Miner. Metall. Mater.* **2015**, *22*, 688.
[31] E. T. Turkdogan, J. V. Vinters, *Metall. Trans.* **1972**, *3*, 1561.
[32] Y. Ma, I. R. Souza Filho, X. Zhang, S. Nandy, P. Barriobero-Vila, G. Requena, D. Vogel, M. Rohwerder, D. Ponge, H. Springer, D. Raabe, *Int. J. Miner. Metall. Mater.* **2022**, *29*, 1901.
[33] A. Meshram, J. Govro, R. J. OMalley, S. Sridhar, Y. Korobeinikov, *Metals* **2022**, *12*, 2026.
[34] A. Meshram, J. Govro, Y. Korobeinikov, S. Chakraborty, R. J. OMalley, in *AISTech - Iron and Steel Technology Conf. Proc.*, AIST, Pittsburgh, PA, May 2022, https://doi.org/10.33313/386/030.
[35] M. Pei, M. Petäjäniemi, A. Regnell, O. Wijk, *Metals* **2020**, *10*, 972.
[36] T. Astoria, *Direct From MIDREX*, Midrex Technologies, Inc., Charlotte, NC **2019**.
[37] B. E. Monsen, E. S. Thomassen, I. Bragstad, E. Ringdalen, P. H. Hoegaas, *AISTech 2015*, Vol. *1*, Cleveland, Oh, May **2015**, p. 11.
[38] L. Yi, Z. Huang, H. Peng, T. Jiang, *J. Cent. South Univ.* **2012**, *19*, 2291.
[39] Q. T. Tsay, W. H. Ray, J. Szekely, *AIChE J.* **1976**, *22*, 1064.
[40] A. Abdelrahim, M. Iljana, M. Omran, T. Vuolio, H. Bartusch, T. Fabritius, *ISIJ Int.* **2020**, *60*, 2206.
[41] E. T. Turkdogan, R. G. Olsson, J. V. Vinters, *Metall. Mater. Trans. B* **1971**, *2*, 3189.
[42] C. Scharm, F. Küster, M. Laabs, Q. Huang, O. Volkova, M. Reinmöller, S. Guhl, B. Meyer, *Miner. Eng.* **2022**, *180*, 107459.
[43] R. C. Gupta, A. A. Shaik, *ISIJ Int.* **2005**, *45*, 408.
[44] S. R. Logan, *J. Chem. Educ.* **1982**, *59*, 279.
[45] Y. Chai, Y. Fan, Z. Li, J. Wu, Y. Zhang, Y. Wang, G. Luo, S. An, *ACS Omega* **2022**, *7*, 7759.
[46] A. Rukini, M. A. Rhamdhani, G. A. Brooks, A. Van Den Bulck, *J. Sustainable Metall.* **2022**, *8*, 1.

 © 2023 Wiley-VCH GmbH

1869344x, 0, Downloaded from https://onlinelibrary.wiley.com/doi/10.1002/srin.202300066 by Missouri University Of Science, Wiley Online Library on [16/08/2023]. See the Terms and Conditions (https://onlinelibrary.wiley.com/terms-and-conditions) on Wiley Online Library for rules of use; OA articles are governed by the applicable Creative Commons License